

Automated fault detection and analysis for large photovoltaic systems using photovoltaic module fault detection in drone vision system

Rotimi-Williams Bello^{1*}, Pius A. Owolawi², Chunling Tu³, Etienne A. van Wyk⁴

^{1,2,3,4}Department of Computer Systems Engineering, Faculty of ICT, Tshwane University of Technology, South Africa; bellorw@tut.ac.za (R.W.B.) owolawipa@tut.ac.za (P.A.O.) duc@tut.ac.za (C.T.) vanwykea@tut.ac.za (E.A.V.W.).

Abstract: This study presents an innovative approach to fault detection in large-scale photovoltaic (PV) systems by leveraging the capabilities of drones and machine vision technologies. The proposed method is unsupervised, eliminating the need for manual intervention in identifying and analyzing faults in PV installations. By employing drone vision techniques equipped with high-resolution cameras and advanced image processing algorithms, comprehensive visual data of solar panels were captured. The collected images were processed for automatic detection and classification of various faults such as cracks, hotspots, and shading issues. The integration of these technologies not only enhances the accuracy of fault detection but also significantly reduces the time and cost associated with traditional inspection methods. This approach ensures the efficient and reliable operation of PV systems, contributing to the sustainable generation of solar energy. The original dataset employed in this work can be found at <https://doi.org/10.17632/5ssmfjgrpc.1>.

Keywords: Cracks, Drone vision system, Hotspots, Inspection efficiency, Photovoltaic systems, Shading.

1. Introduction

The implementation of drones equipped with thermal and optical sensors has revolutionized the inspection process, allowing for comprehensive, rapid, and cost-effective monitoring of expansive solar fields. Moreover, the global demand for renewable energy has spurred the rapid expansion of photovoltaic (PV) systems, making solar power one of the fastest-growing sources of electricity [1]. As PV installations scale up in size and number, the need for efficient and effective monitoring and maintenance of these systems becomes increasingly important [2]. Traditional inspection methods, often manual and labor-intensive, are not only time-consuming but also pose significant challenges in terms of accuracy and consistency, particularly in large-scale deployments [3]. To address these challenges, there is a growing interest in leveraging advanced technologies such as drones and machine vision [4]. In the pursuit of enhancing the reliability and efficiency of PV systems, the integration of drones and machine vision technologies for unsupervised fault detection has emerged as a promising frontier.

Drones offer a flexible and cost-effective platform for data collection, capable of capturing high-resolution images of vast PV arrays in a fraction of the time required by ground-based inspections [5]. When combined with machine vision algorithms, these images can be processed and analyzed to detect and classify faults autonomously, without the need for human oversight [6, 7]. There are numerous studies that have utilized the techniques of image processing for the detection and analyses of large PV systems faults [8]. Different advanced imaging sensors-based UAV devices have been used to capture high-resolution PV panel images [9]. To get the data ready for additional analysis, these images go through different preprocessing stages, which include reduction of noise, enhancement of contrast, and normalization [10].

Faults in PV systems can be detected primarily by identifying the different anomalies such as cracks, hotspots, and shading effects in the images [11]. Different algorithms of machine vision have also been applied to highlight these anomalies, specifically, techniques like histogram equalization and thresholding are utilized to ameliorate the visibility of possible faults, before applying image segmentation to isolate areas of interest, facilitating targeted analysis [12]. After completing the segmentation, analysis of each segment is followed by pattern recognition and algorithms of classification to establish the fault and its type. The design of the system is such that it works without being supervised, using models of machine learning that are trained on various datasets of labeled anomalies. With this approach, the detected faults can be classified automatically without manual support, and thus meaningfully optimizing the maintenance time and efforts [13]. Researchers have implemented video processing that aids in understanding the health of PV systems [14] whereby continuous footage of solar panels is captured by quadcopter equipped with video cameras.

Frame-by-frame, the captured solar panels are then processed for the detection of dynamical changes and invisible faults in static images [15]. The workflow of the video processing is by extraction of video feed's key frames, concentrating on frames with substantial changes or possible faults, and the processing of these key frames is by similar techniques of image processing [16]. However, temporal changes analysis is also allowed by video processing, such as hotspots progression or shading widespread over time [17]. The process for fault detection is enhanced by using motion detection and algorithm for tracking to monitor anomalies across multi-frames [18]. By this, the faults development and the impact on the PV system overall performance can be monitored by the system. By combining image and video processing, there is an assurance of a more accurate and robust mechanism for detecting faults [19].

In furtherance of the existing related work, this paper explores the application of an unsupervised fault detection system that integrates drone-based imaging and machine vision for large PV systems. It delves into the intricate dynamics of large PV systems, employing state-of-the-art image processing techniques and machine learning algorithms to detect and analyze faults in an unsupervised manner. The work in this study is a step towards developing a method that can identify various types of faults, such as cracks, hotspots, and shading, with high accuracy and minimal human intervention. By enhancing the efficiency and reliability of PV system maintenance, the approach contributes to the sustainable and uninterrupted operation of solar power plants, for a more resilient and greener energy grid.

2. Materials and Methods

The main hardware components that comprise the materials employed in carrying out the experiment in this study are DJI Mavic 3 Thermal drone, solar panels, PV modules, inverter, storage battery, DC load, and solar charge controller. The main software materials are Windows 11 Home, Open CV, Python 3.x with libraries such as Flask, NumPy, and Matplotlib, computer vision algorithms with edge detection algorithm, morphological operations, and feature extraction algorithm plus the techniques of histogram equalization and thresholding.

2.1. Application of Image Processing

This study foundation lies in utilizing the techniques of image processing for detecting and analyzing large PV systems faults. Advanced imaging sensors-based drones are employed in capturing PV panel images of high-resolution. To get the data ready for additional analysis, these images go through different preprocessing stages, which include reduction of noise, enhancement of contrast, and normalization. PV faults are normally detected by identifying anomalies such as cracks, hotspots, and shading effects in the images, and these anomalies are highlighted by employing the algorithms of machine vision, including detection of edge, morphological operations, and extraction of features. Specifically, potential faults are made visible by histogram equalization technique, thresholding technique, etc. [20]. Areas of interest are then isolated by image segmentation, through which analysis

of the target is facilitated. After completing the segmentation, analysis of each segment is followed by pattern recognition and algorithms of classification to establish the fault and its type. The design of the system is such that it works without being supervised, using models of machine learning that are trained on various datasets of labeled anomalies. With this approach, the detected faults can be classified automatically without manual support, and thus meaningfully optimizing the maintenance time and efforts. Figure 1 shows the system description.

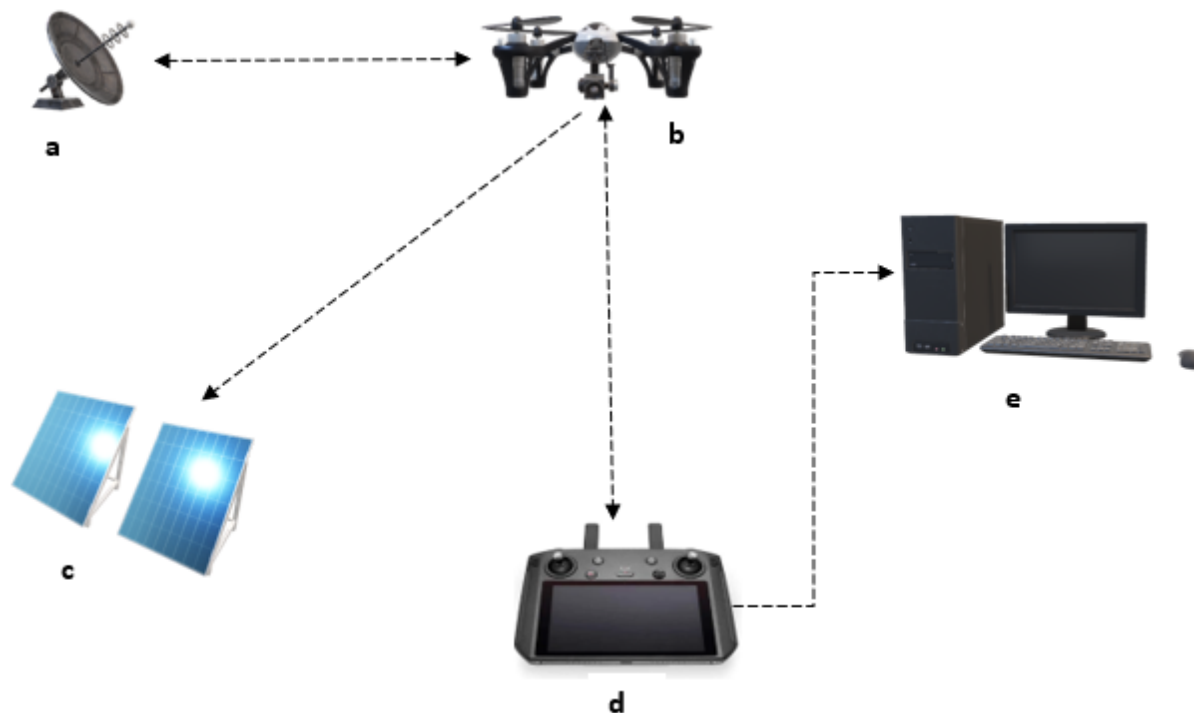


Figure 1. System description showing (a) Satellite (b) DJI Mavic 3 Thermal drone (c) Solar PV (d) Remote control (e) PC [21].

2.2. Application of Video Processing

To provide a complete overview of the health of the PV system, video processing is implemented in addition to image processing. The solar panels' continuous footage is captured by video camera-embedded drones. Frame-by-frame, the captured solar panels are then processed for the detection of dynamical changes and invisible faults in static images. The workflow of the video processing is by extraction of video feed's key frames, concentrating on frames with substantial changes or possible faults, and the processing of these key frames is by similar techniques of image processing. However, temporal changes analysis is also allowed by video processing, such as hotspots progression or shading widespread over time. The process for fault detection is enhanced by using motion detection and algorithm for tracking to monitor anomalies across multi-frames. By this, the faults development and the impact on the PV system overall performance can be monitored by the system. By combining image and video processing, there is an assurance of a more accurate and robust mechanism for detecting faults.

As shown in Figure 1, the detailed images and videos of a solar PV array are captured by the deployed thermal camera-embedded DJI Mavic 3 drone. The drone flies over the installed solar, analytically gathering visual data that shows the PV panels' thermal characteristics. This data comprises images and videos, which are then moved to a computer for processing by specialized application. The thermal data are analyzed during the processing for the detection of anomalies, which

are indicative of solar panels faults. This method presents a complete and effective approach for large PV systems monitoring and maintenance. Figure 2 shows the workflow of the proposed system.

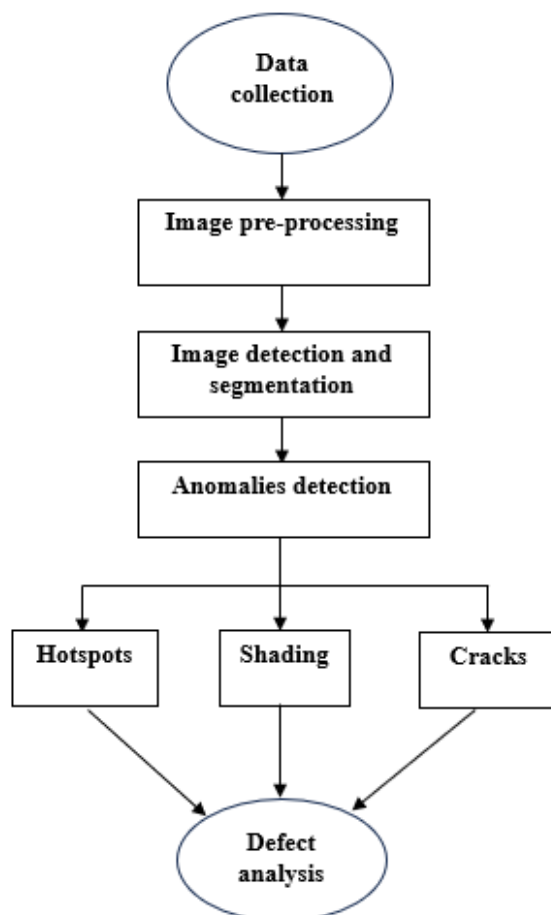


Figure 2.
Workflow of the proposed systems.

As shown in Figure 2, drone was employed and hovered over the PV modules to start capturing thermal data. The thermal camera-embedded drone records the solar panels' conditions. PV array's thermal images and videos are captured by the drone, including gathering of complete data on the external temperature and possible anomalies across the solar panels. After data collection, the thermal images and videos are transmitted by the drone to a computer for more processing and analysis. The transmitted data go through preprocessing stages like reduction of noise and normalization for the enhancement of the images and videos' quality and clarity, thereby enabling their suitability for analysis. The pre-processed data are handled by the algorithms of machine vision for anomalies detection, such as hotspots, cracks, or shading, that might be indicative of PV panels' faults. The detected faults are evaluated at the analysis stage, the types of the detected faults and their exact locations on the solar panels are also determined and pinpointed at this stage.

2.3. Tools for Enhancing Visual Data Captured by Drones

Morphological transformation operations and canny edge algorithms are the essential tools used for the enhancement of visual data captured by the drones.

2.3.1. Morphological Transformation

Morphological transformation operations are essential tools for enhancing the visual data captured by drones [22]. When monitoring PV systems, the images or videos obtained often contain noise and artifacts that can obscure the detection of faults like cracks, hotspots, or shading. Morphological operations help refine the images, making the analysis more accurate [23]. The application of the operations is as follows:

- a) Dilation: This operation can be used to emphasize or connect small features in the images, such as cracks or edges of hotspots, making them more detectable by subsequent processing steps.
- b) Erosion: By applying erosion, the algorithm can reduce noise and eliminate small, irrelevant details that might interfere with the accurate detection of faults.
- c) Opening and closing: These operations are combinations of dilation and erosion that help in cleaning up the images further. Opening can be particularly useful for removing small objects or noise, while closing is effective for filling in small holes or gaps within larger objects, such as minor discontinuities in panel surfaces.

2.3.2. Canny Edge Algorithm

The Canny edge algorithm is a powerful technique used for detecting edges in images with high precision [24]. In the context of PV system monitoring, this algorithm is instrumental in identifying the boundaries of various faults, such as cracks or physical defects on the panels [25]. The application of the algorithm of Canny edge is as follows:

- a) Edge detection: The Canny algorithm detects the edges of anomalies by identifying points of sharp intensity changes in the images. This is critical for isolating faults, as it allows the detection system to focus on the exact locations where the panel's structure is disrupted.
- b) Noise reduction: By incorporating a Gaussian blur in the initial step, the Canny algorithm helps reduce the impact of noise on the edge detection process, ensuring that only significant edges (faults) are identified.
- c) Non-maximum suppression and thresholding: These steps ensure that the detected edges are precise and distinct, minimizing false positives. This precision is essential for accurately pinpointing defects on the PV panels, which can then be addressed through maintenance. In essence, the Canny edge algorithm provides a robust and reliable method for detecting the exact boundaries of faults in PV panels, enabling precise and targeted maintenance efforts. This ensures the efficient operation of large-scale PV systems, as identified issues can be promptly addressed, minimizing downtime and maximizing energy production. Figure 3 shows the usefulness of morphological operation and Canny edge algorithms as tools for enhancing the visual data captured by drones.

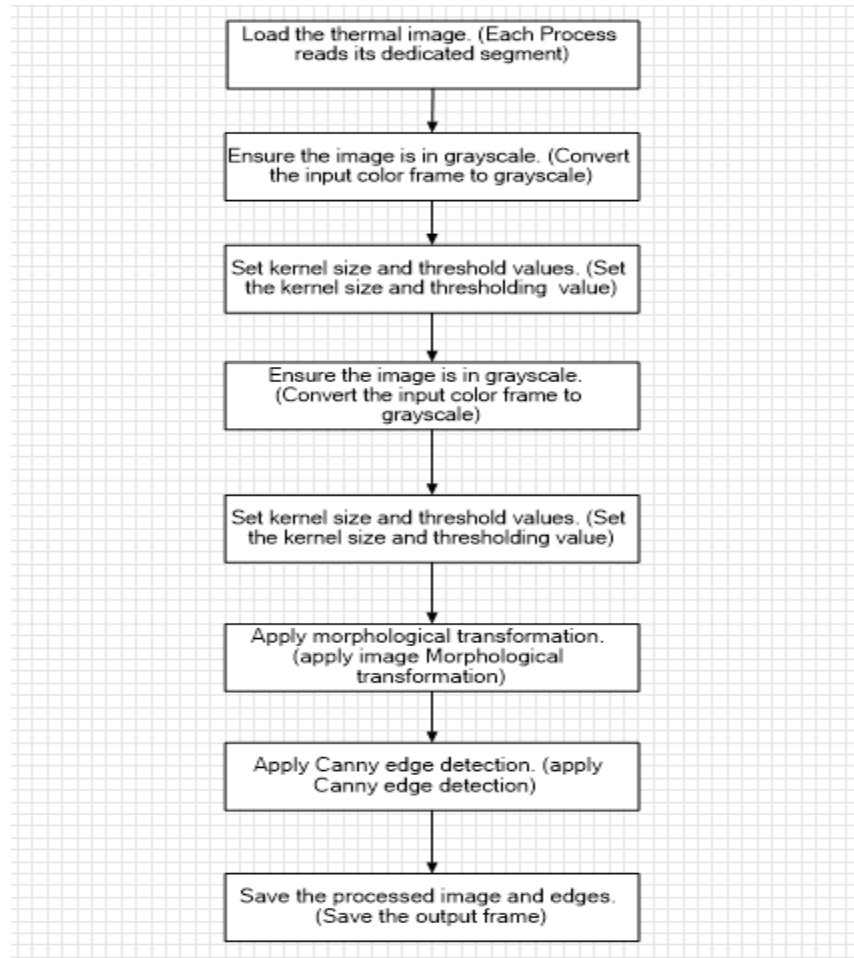


Figure 3. Operational sequence of morphological operation and Canny edge algorithms as tools for enhancing the visual data captured by drones.

2.4. Segmentation Based on Hot Pixels Seeds

Segmentation based on hot pixel seeds using various algorithms helps enhance and accurately detect anomalies in images of PV systems. Here, we provide an overview of the algorithms mentioned, explain their process, and illustrate how they might integrate with machine learning for segmentation.

2.4.1. Box Blur

Box blur, also known as a mean filter, averages the pixels within a kernel or window around each pixel in an image. This reduces image noise and smooths the image, which can help in reducing false positives when detecting hot pixels. In a machine learning context, a box blur might be used in a pre-processing pipeline to smooth images before feeding them into a neural network or other machine learning models. For a given pixel (i,j) , the output pixel value after box blur is given as illustrated by Equation (1):

$$I_{\text{blur}}(i, j) = \frac{1}{K} \sum_m^{\frac{K}{2}} = -\frac{K}{2} \sum_n^{\frac{K}{2}} = -\frac{K}{2} I(i + m, j + n) \quad (1)$$

where,

I is the input image.

K is the total number of pixels in the kernel.

k is the size of the kernel.

2.4.2. Gaussian Blur

Gaussian blur uses a Gaussian function to calculate the transformation of each pixel, effectively smoothing the image and reducing noise while maintaining edge integrity better than the box blur. The Gaussian blur of an image is given as illustrated by Equation (2):

$$I_{\text{blur}}(i, j) = \frac{1}{K} \sum_m^{\frac{K}{2}} = -\frac{K}{2} \sum_n^{\frac{K}{2}} = -\frac{K}{2} G(m, n) \cdot I(i + m, j + n) \quad (2)$$

where,

$$G(m, n) = \frac{1}{2\pi\sigma^2} e^{-\frac{m^2 + n^2}{2\sigma^2}}$$

σ is the standard deviation, determining the spread of the blur.

2.4.3. Median Blur

Median blur replaces each pixel with the median of the surrounding pixel values. This is particularly useful for removing salt-and-pepper noise while preserving edges. The output of the median blur for a given pixel (i,j) is illustrated by Equation (3):

$$I_{\text{blur}}(i, j) = \text{Median}(\{ I(i + m, j + n) \mid m, n \in \text{Kernel} \}) \quad (3)$$

2.4.4. Histogram Equalization

Histogram equalization enhances the contrast of an image by spreading out the most frequent intensity values, making it easier to identify features such as hot pixels. The formula for histogram equalization is illustrated by Equation (4):

$$I_{\text{eq}}(i, j) = \text{floor} \left(\frac{(L - 1) \times \text{CDF}(I(i, j))}{\text{Total Pixels}} \right) \quad (4)$$

where,

L is the number of intensity levels.

CDF is the cumulative distribution function of the intensity histogram.

2.4.5. Segmentation Based on Hot Pixels Structured

The workflow and flowchart of the segmentation process based on hot pixels structured are presented in this section.

A) Workflow

Start

Initiate the segmentation process

Load input image

Load the original image that needs to be processed

Preprocessing technique selection

Decision point: Choose a preprocessing technique

If box blur:

Apply box blur to the image

$$\text{Box blur}(I) = \frac{1}{N^2} \sum_{i=-k}^k \sum_{j=-k}^k I(x+i, y+j)$$

Subtract the blurred image from the original

$$\text{Diff}_{\text{Box}}(x, y) = I(x, y) - \text{Box blur}(I(x, y))$$

Highlight hot pixels where $\text{Diff}_{\text{Box}}(x, y) > T$ (where T is a threshold)

If Gaussian blur:

Apply Gaussian blur to the image

$$\text{Gaussian blur}(I) = \frac{1}{2\pi\sigma^2} e^{-\frac{x^2+y^2}{2\sigma^2}}$$

Subtract the blurred image from the original

$$\text{Diff}_{\text{Gaussian}}(x, y) = I(x, y) - \text{Gaussian Blur}(I(x, y))$$

Identify hot pixels where $\text{Diff}_{\text{Gaussian}}(x, y) > T$

If histogram equalization:

Apply histogram equalization to the image

$$\text{Ieq}(x, y) = \text{HE}(I(x, y))$$

Enhance contrast to facilitate hot pixel detection

$$\text{Diff}_{\text{HE}}(x, y) = \text{Ieq}(x, y) - I(x, y)$$

Highlight hot pixels where $\text{Diff}_{\text{HE}}(x, y) > T$

If Median blur:

Apply median blur to the image

$$\text{Median blur}(I(x, y)) = \text{Median}\{I(x+i, y+j)\}$$

Compare the blurred image to the original.

$$\text{Diff}_{\text{Median}}(x, y) = I(x, y) - \text{Median blur}(I(x, y))$$

Find hottest pixel

Calculate the hottest pixel value

$$\text{Hot}_{\text{pixel}} = \max_{(x,y)} I(x, y)$$

Determine the location of the hottest pixel

Generate output and graph

Output the processed image with hot pixels identified

Display the hottest pixel value and location

Generate a graph visualizing the pixel intensities

Graph = $\{(x, y, I(x, y)) | (x, y) \in \text{Image dimensions}\}$

Combine and validate hot pixels

Collect potential hot pixels from all methods

Cross-validate and refine the selection

Validated hot pixels = \bigcup Hot pixels from all methods

Segmentation

Segment the image based on validated hot pixels

Segmented image = $\{ I(x, y) \in \text{Validated Hot Pixels} \}$

Mark regions containing hot pixels

Output segmented Image

Produce the final segmented image with hot pixels identified

End

Conclude the segmentation process

B) Flowchart

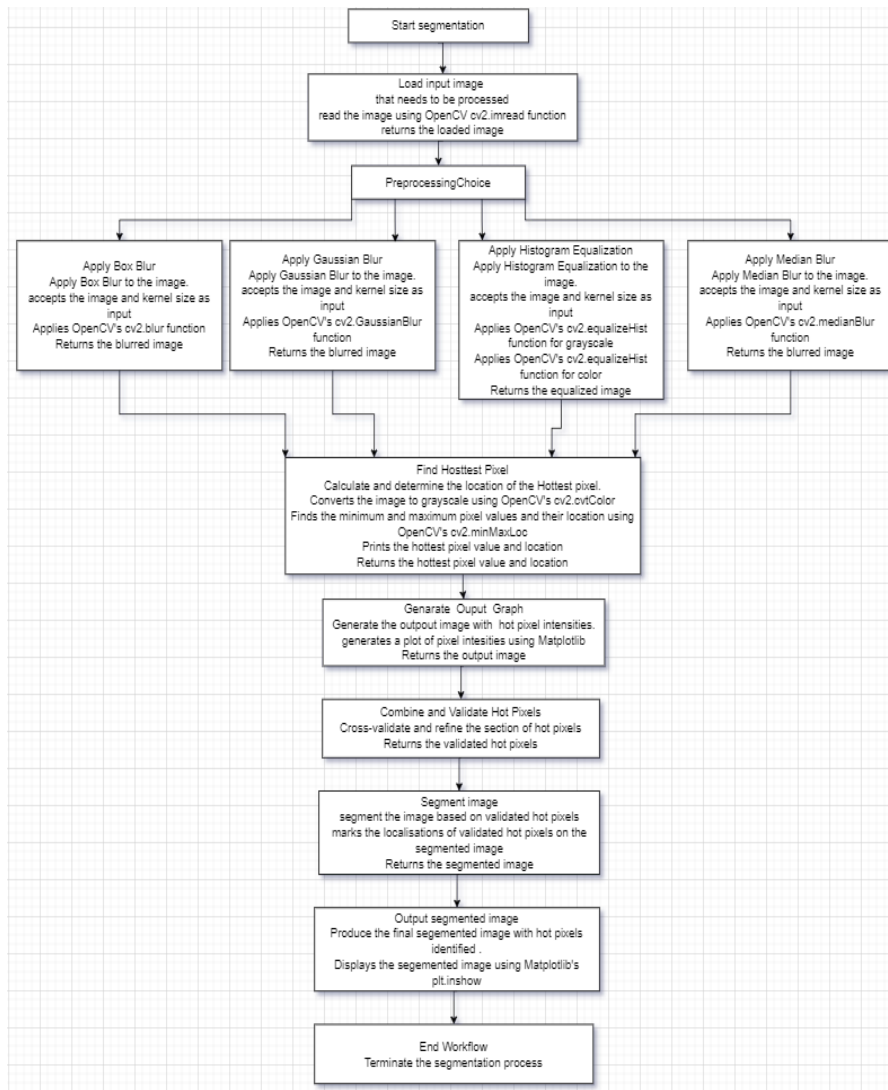


Figure 4.
Segmentation based on hot pixels seeds.

Hot pixel spots in the context of solar PV systems can be dangerous for several reasons, among which are:

- a) Heat accumulation: Hot pixel spots on solar panels indicate localized areas where the panel is absorbing more sunlight and converting it into heat rather than electricity.
- b) Reduced efficiency: Solar panels are designed to convert sunlight into electrical energy efficiently.
- c) Cell degradation: Prolonged exposure to hotspots can accelerate the degradation of solar cells.
- d) Potential for cell failure: Hotspots can create thermal stress on the solar cells, increasing the risk of cell failure or permanent damage.
- e) Fire hazard: In extreme cases, particularly with concentrated hotspots, there is a risk of fire hazard.
- f) Impact on system performance: Beyond affecting individual panels, hotspots can impact the performance of the entire solar PV system.

3. Implementation

For the validation of our proposed work, we collected images in the Digital Image and Signal Processing (DISPLAY) lab at Tshwane University of Technology (TUT) for our remote PV system. The system includes two panels of Jinko JKM200M-72 modules, each producing 200 W. The PV modules' main specifications in the DISPLAY lab are shown in Table 1. The entire system was assembled in our lab, ensuring all required components, connections, measurements, and mounting were carefully managed.

Table 1.
System specifications of the JKM200M-72 module.

Electrical specification (Nominal)	
Max power	200 W
Open circuit voltage	45.6 V
Short circuit current	5.8 A
Maximum power voltage	36.9 V
Maximum power current	5.42 A
Maximum series fuse current	10 A
Maximum system voltage	1000 V
Mechanical specifications	
Cells	72
Module dimensions	62.2 × 31.8 in.
Module thickness	1.4 in.
Weight	32 lb
Limits	
Temperature of operating module	-40°F to +185°F
Storm resistance/Static load	Tested to IEC 61215 for loads of 5400 Pa (113 psf)

The PV system's schematic diagram is illustrated in Figure 5, while the complete installed system in DISPLAY is shown in Figure 6. Alongside our collected data, we also utilized images of PV modules taken at the Soshanguve South campus of TUT during drone flyovers. Additionally, we included images sourced online, used with permission.

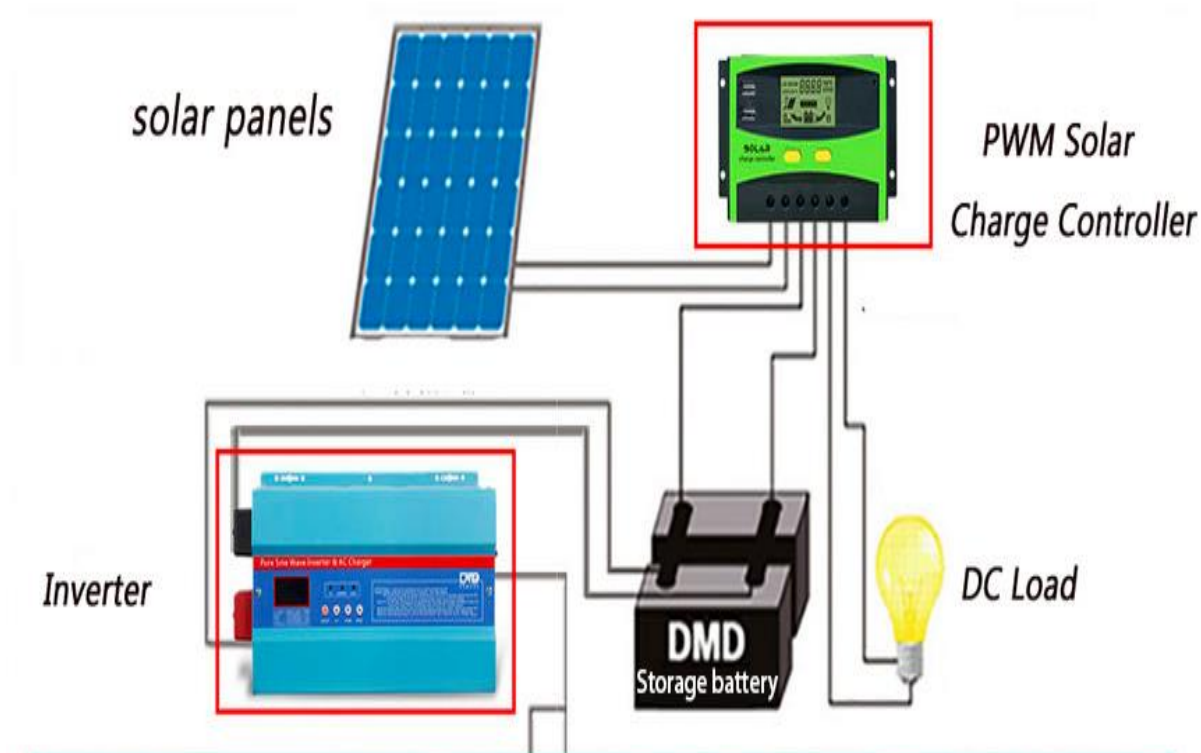


Figure 5.
Schematic diagram of stand-alone trolley PV solar.

The DJI Mavic 3 Thermal is a state-of-the-art drone specifically designed for thermal imaging and inspection tasks, offering a suite of advanced features ideal for detailed analysis of PV systems. Below are the key specifications that underscore its capabilities:

3.1. DJI MAVIC 3 Thermal Specifications

a) Thermal Imaging Camera:

Resolution: 640×512 pixels

Frame rate: 30 Hz

Field of view (FOV): $61^\circ \times 47^\circ$

Thermal sensitivity (NETD): ≤ 50 mK at f/1.0

Temperature measurement range: -20°C to 150°C , 0°C to 500°C (High gain mode)

Image processing enhancements: Features integrated with advanced image processing technologies, including MSX for enhanced image detail.

b) Visual Imaging Camera:

Sensor: 1/2" CMOS, 12 MP

Video resolution: Up to 4K (3840×2160) at 30fps

Field of view (FOV): 56° horizontal

Digital zoom: Capable of up to $32\times$ digital zoom for close inspection.

c) Flight Performance:

Maximum flight time: Approximately 45 minutes under optimal conditions.

Maximum speed: 72 km/h in sport mode.

Maximum transmission distance: 15 km, supported by the O3+ transmission system.

Obstacle detection: Provides omnidirectional sensing (forward, backward, upward, downward, and lateral) for enhanced flight safety.

d) Drone Design:

Weight: Approximately 920 grams.

Dimensions: 221 × 96.3 × 90.3 mm (folded), 347.5 × 283 × 107.7 mm (unfolded).

e) Additional Features:

Satellite navigation: Supports GPS, GLONASS, and Galileo.

RTK compatibility: Optional integration with the D-RTK 2 Mobile Station for enhanced positioning accuracy.

Intelligent flight modes: Includes smart tracking, waypoint flight, and AI spot-check for efficient and automated inspection processes.

The capabilities of the DJI Mavic 3 Thermal's high-resolution thermal and visual imaging, in addition to its advanced flight features, make it an exceptional tool for efficient and precision PV systems inspections. Its modern design and portability further distinguish it from other thermal imaging solutions, such as the FLIR Vue Pro, by providing a comprehensive and versatile inspection platform.

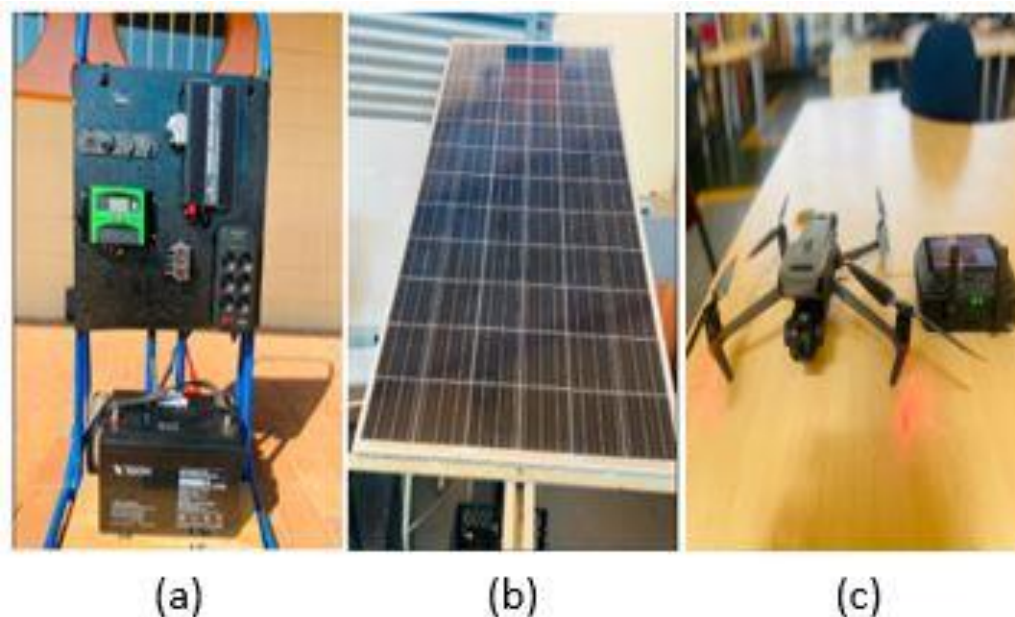


Figure 6.

In the DISPLAY Lab at TUT showing implemented (a) PV module (b) Solar panels (c) DJI Mavic 3T equipped with an integrated thermal camera [26]

In the DISPLAY lab, the system's external defects were simulated by placing polystyrene materials at the back of the PV panel, adhesive paper on the front glass, and a small piece of gum. To further test the system, an input image from an online source was also utilized. Thermal and visual data were processed by utilizing Python 3.x, Windows 11 Home environment, Intel Core i5-4210M CPU @ 2.60 GHz, and 8 GB of RAM. The images were processed and analyzed by OpenCV, Python, with libraries such as Flask, NumPy, and Matplotlib. The pip commands were used for the installation of libraries, accelerating the implementation of image processing tasks, such as thermal anomaly detection.

4. Results and Discussions

This section presents and discusses the results obtained from the experiment carried out in this study. Figure 7 illustrates the interface of the PV module fault detection and demonstrates its functionality with images.

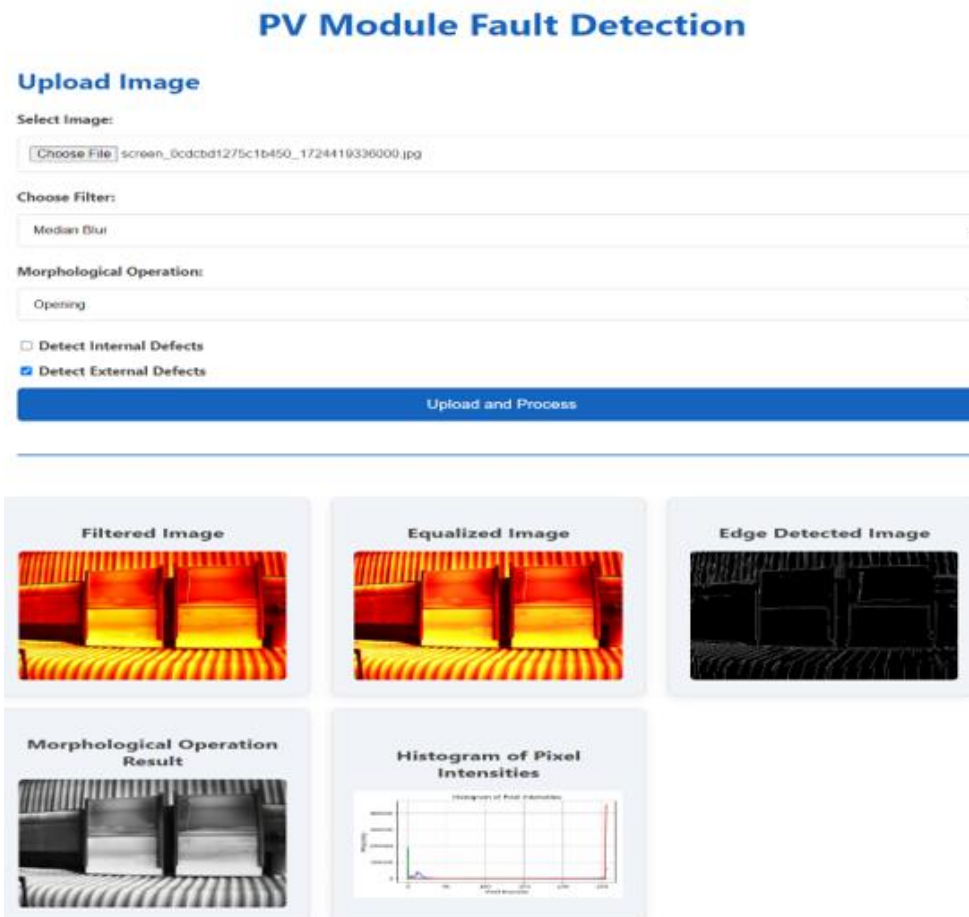


Figure 7. Illustration of application's interface, demonstrating its functionality with images.

4.1. Effects of Morphological Transformations and Canny Edge Detector

The implementation of morphological transformations and canny edge detector was for the hotspots detection in the PV module. As illustrated in Figure 8, the thermal image was processed using the following techniques to enhance and detect hotspots:

(a) Filtered image: The initial raw thermal image was subjected to a box blur filter, which smooths the image and reduces noise, preparing it for further analysis.

(b) Equalized image: Following filtering, histogram equalization was applied to the image. This step improves contrast, making features more distinct and easier to analyze.

(c) Edge-detected image: The contrast-enhanced image was then processed using the Canny edge detector, which highlights the edges and boundaries within the image, revealing potential hotspots.

(d) Morphological operation result (Dilation): Finally, a morphological dilation operation was performed on the edge-detected image. This technique expands the detected edges, making them more prominent and continuous, thus facilitating better identification of significant features.

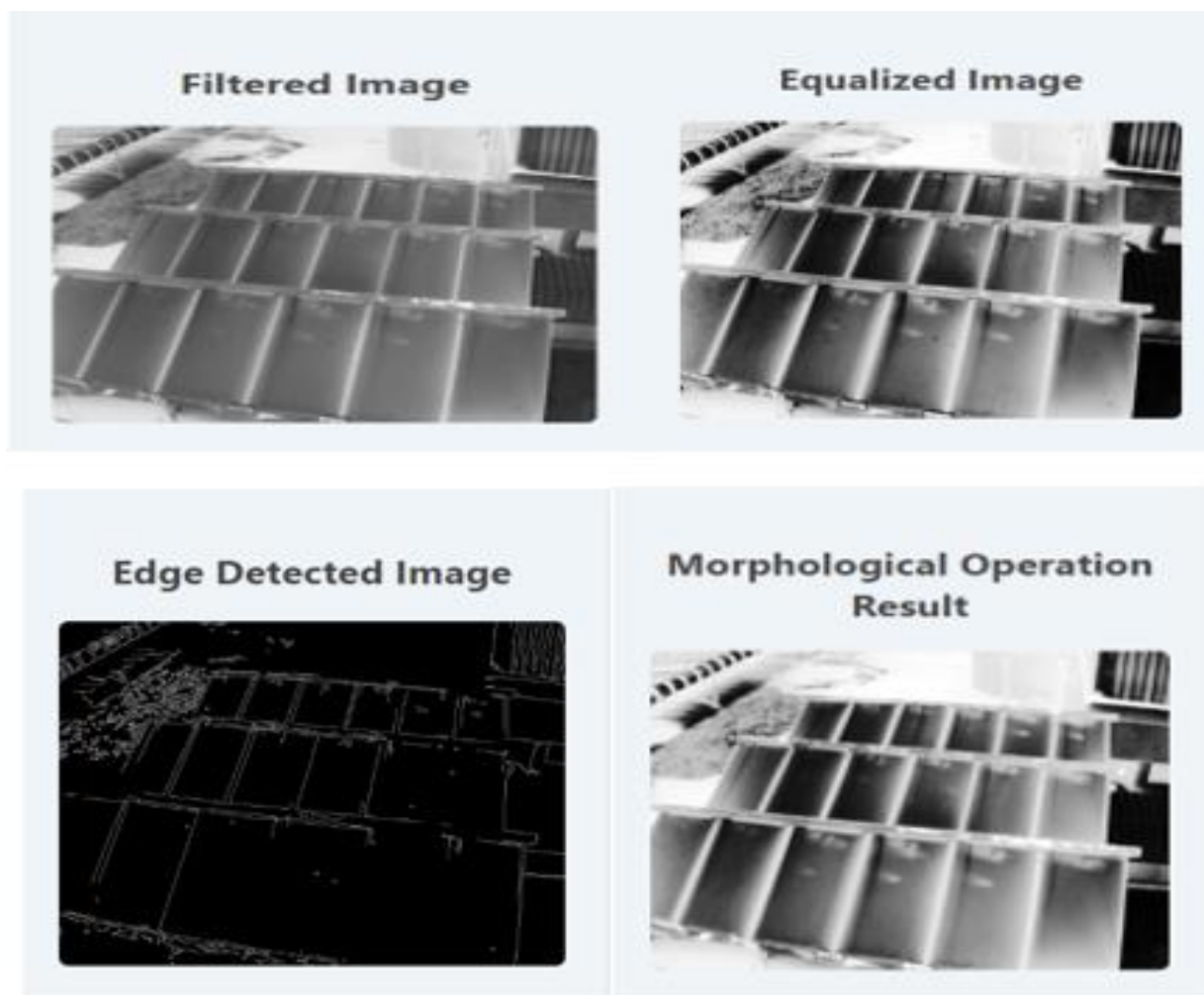


Figure 8. Enhancement and detection of hotspots using filtered image, equalized image, edge detected image, and dilation.

4.2. Effects of Gaussian Blur and Morphological Erosion

The segmentation of thermal hotspots in the PV module was achieved using Gaussian blur and morphological erosion, alongside the Canny edge detector, as illustrated in Figure 9. To effectively identify hotspots in thermal images, we applied a series of sophisticated image processing methods:

(a) Initial filtering: We started with the raw thermal image and applied Gaussian blur to it. This step smooths out the image and reduces noise, which prepares the image for clearer subsequent processing.

(b) Contrast enhancement: Next, we enhanced the image's contrast using histogram equalization. This adjustment makes the features in the image stand out more sharply, facilitating better detection of thermal anomalies.

(c) Edge detection: With the enhanced image, we used the Canny edge detection algorithm. This technique highlights the edges and boundaries within the image, revealing the contours of potential hotspots.

(d) Morphological refinement (Erosion): Finally, we performed morphological erosion on the edge-detected image. Erosion helps to eliminate small unwanted details and noise, refining the edges to better delineate the significant thermal features and improve the accuracy of hotspot detection. These steps

together provide a comprehensive approach to analyzing thermal images, ensuring precise identification and evaluation of hotspots.

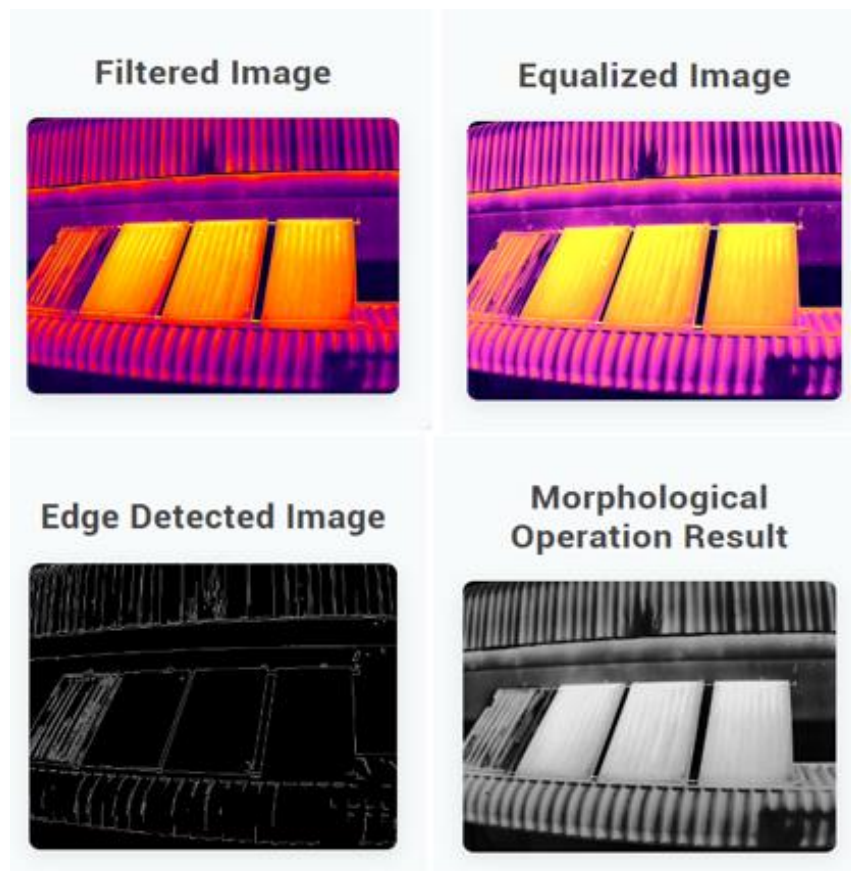


Figure 9. The segmentation of thermal hotspots in the PV module using Gaussian blur and morphological erosion, alongside the Canny edge detector.

Figure 10 presents the pixel intensity graph generated from the processed thermal image utilizing the described techniques. This graph offers an in-depth view of how pixel intensities are distributed throughout the image, which is essential for analyzing thermal anomalies. By applying morphological refinement through erosion, the graph highlights the refined intensity patterns, making it easier to identify and assess significant thermal features and anomalies.

Histogram of Pixel Intensities

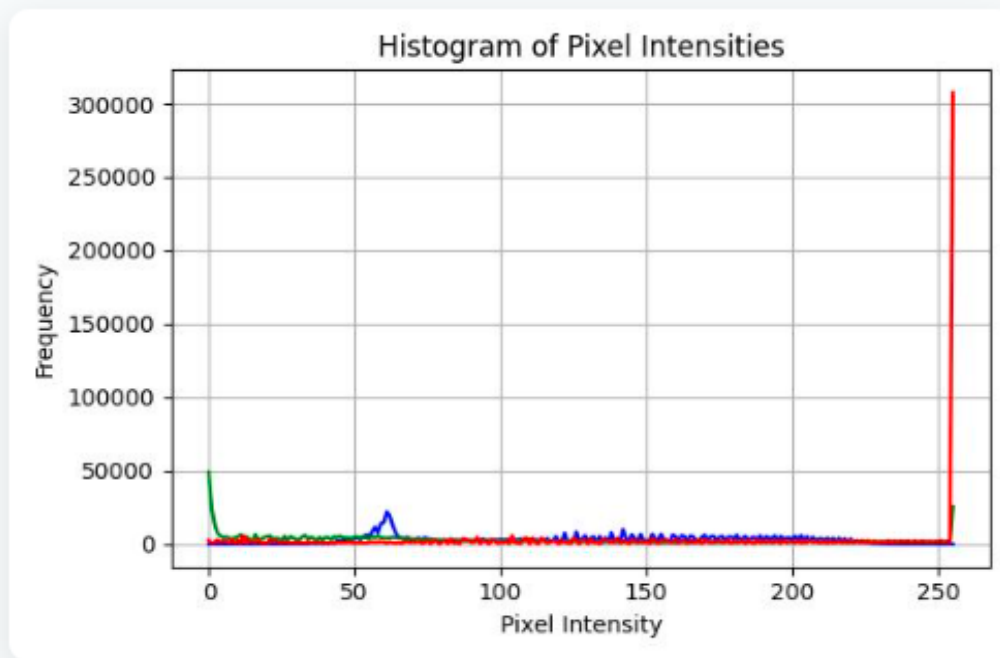


Figure 10.
Histogram of pixel intensities.

Figure 11 demonstrates the detection of simulated defects on the PV module. To mimic a small external defect, a piece of gum was placed on the glass surface of the module, which was identified as a hotspot. Additionally, a small piece of polystyrene was positioned behind the panel and glued to its back surface. Both the gum on the glass and the polystyrene on the back of the panel were successfully detected, highlighting the system's ability to identify various thermal anomalies.

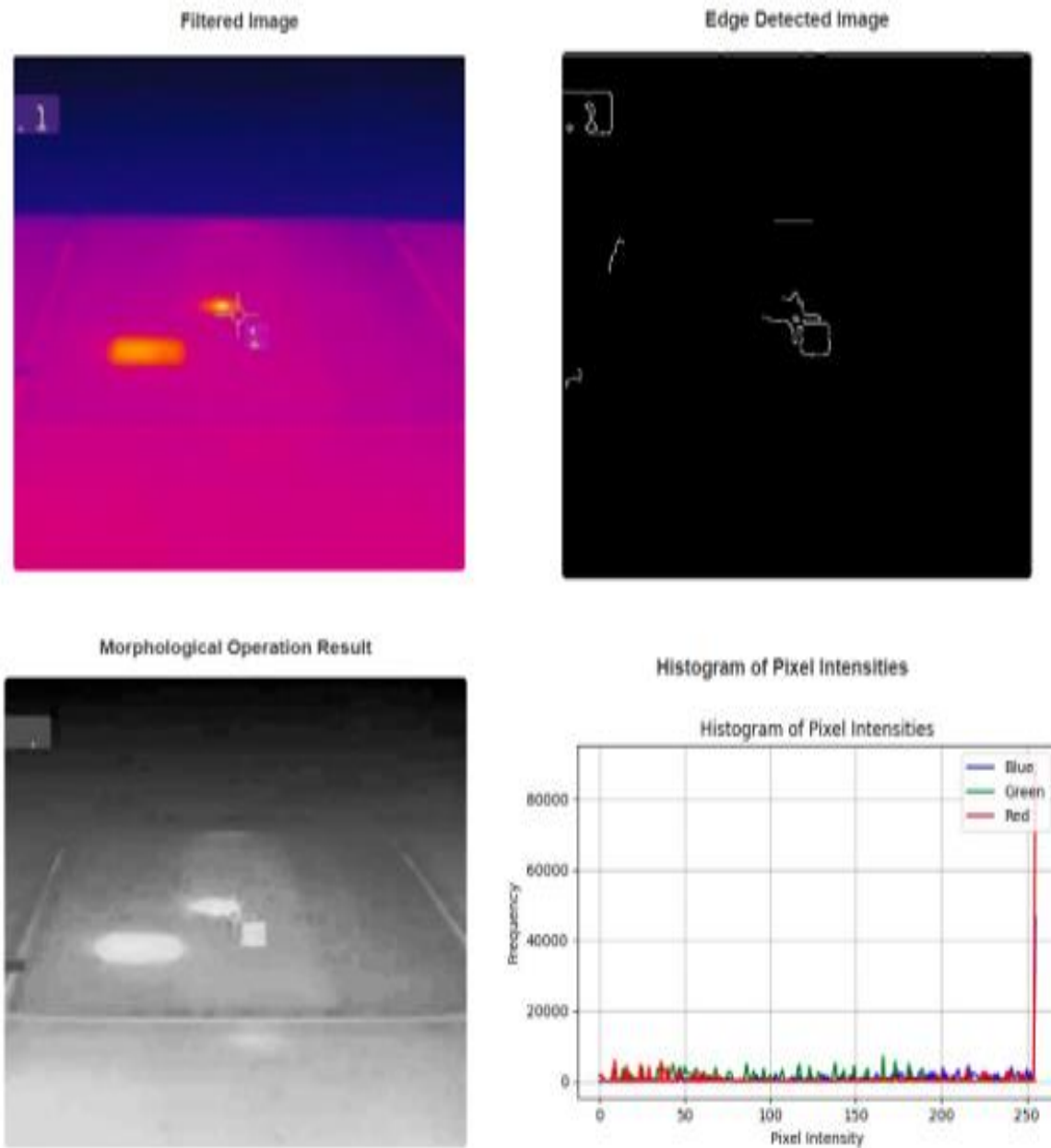


Figure 11.
Demonstration of detection of simulated defects on the PV module.

An input thermal image, obtained with permission from an online source [13] was used to evaluate the effectiveness of the detection algorithms. This image contains PV modules with known defects and was specifically chosen to test the fault detection capabilities of the applied algorithms. Figure 12 presents the results, showcasing how the algorithms successfully identified the defects in the PV modules from the input image.

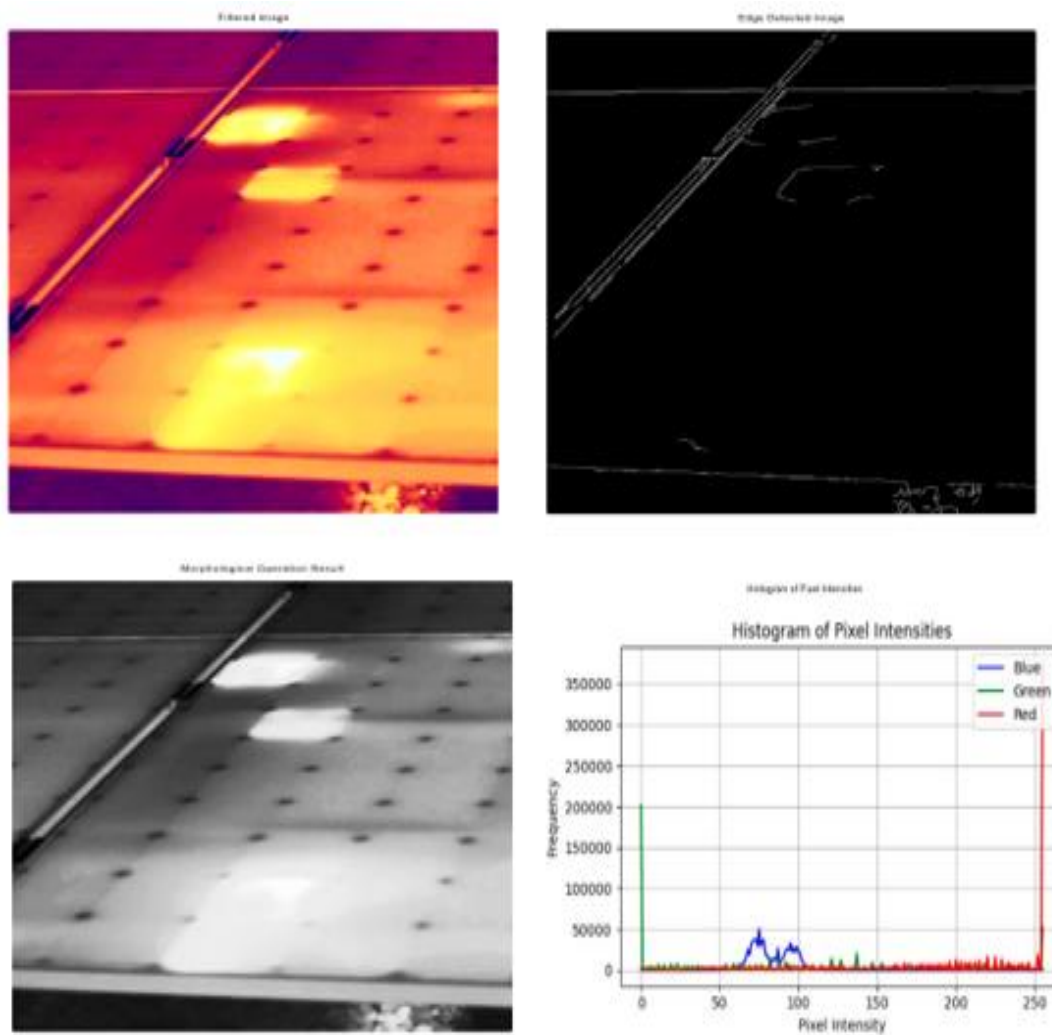


Figure 12.
Result showcasing how the algorithms successfully identified the defects in the PV modules from the input image.

Figure 13 illustrates the pixel intensity graph derived from the processed thermal image using the described techniques. The graph provides a detailed view of the distribution of pixel intensities across the image, which is crucial for analyzing thermal anomalies.

Histogram of Pixel Intensities

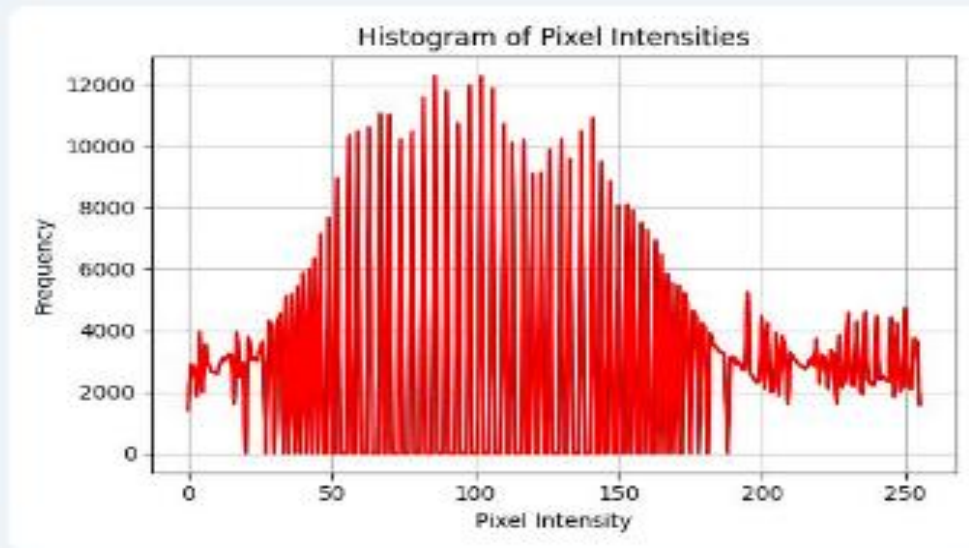
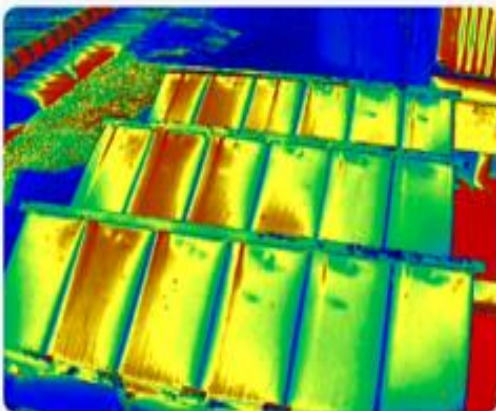


Figure 13:
Illustration of the pixel intensity graph derived from the processed thermal image.

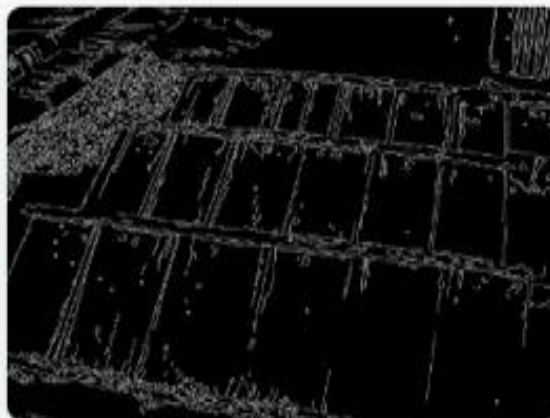
4.3. Effects of Opening Techniques

The opening operation is a morphological transformation used in image processing to clean up small objects or noise from an image. The combination of these two operations, first erosion and then dilation, makes the opening operation particularly effective at removing small, unwanted features while preserving the shape and structure of larger, relevant objects in the image. This is useful in scenarios like image preprocessing, where the goal is to clean up the image before further analysis, such as detecting larger features or objects. Figure 14 illustrates the application of the morphological transformation known as "Opening" within the fault detection process. This operation, consisting of erosion followed by a dilation, effectively removes small objects or noise from the image. In the context of PV system analysis, the opening operation helps in eliminating minor artifacts and irrelevant details, thus enhancing the visibility of significant features such as cracks, hotspots, or other structural anomalies in the PV modules. By cleaning up the image, opening ensures that the subsequent analysis focuses on more prominent and relevant faults, improving the overall accuracy of the fault detection process.

Equalized Image



Edge Detected Image



Morphological Operation Result



Histogram of Pixel Intensities

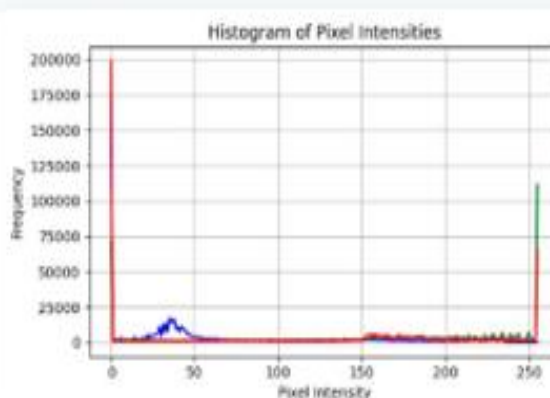


Figure 14.

Application of morphological transformation known as "Opening" within the fault detection process.

4.4. Effects of Closing Techniques

The closing operation, as shown in Figure 15, is a morphological transformation that involves performing a dilation followed by erosion. This operation is particularly useful in the context of image processing for PV systems, where it helps to fill in small gaps, holes, or discontinuities within larger objects. In the context of fault detection for PV modules, the closing operation smooths the contours of detected features, connects adjacent broken parts of a fault, and fills in small cracks or gaps that may have appeared due to noise or imaging artifacts. For example, in thermal images of PV modules, there may be small gaps within regions that should be uniformly hot due to faults like hotspots. The closing operation can fill these gaps, making the fault areas more coherent and easier to detect. This enhances

the accuracy of fault detection by ensuring that minor discontinuities do not lead to missed or fragmented fault detection.

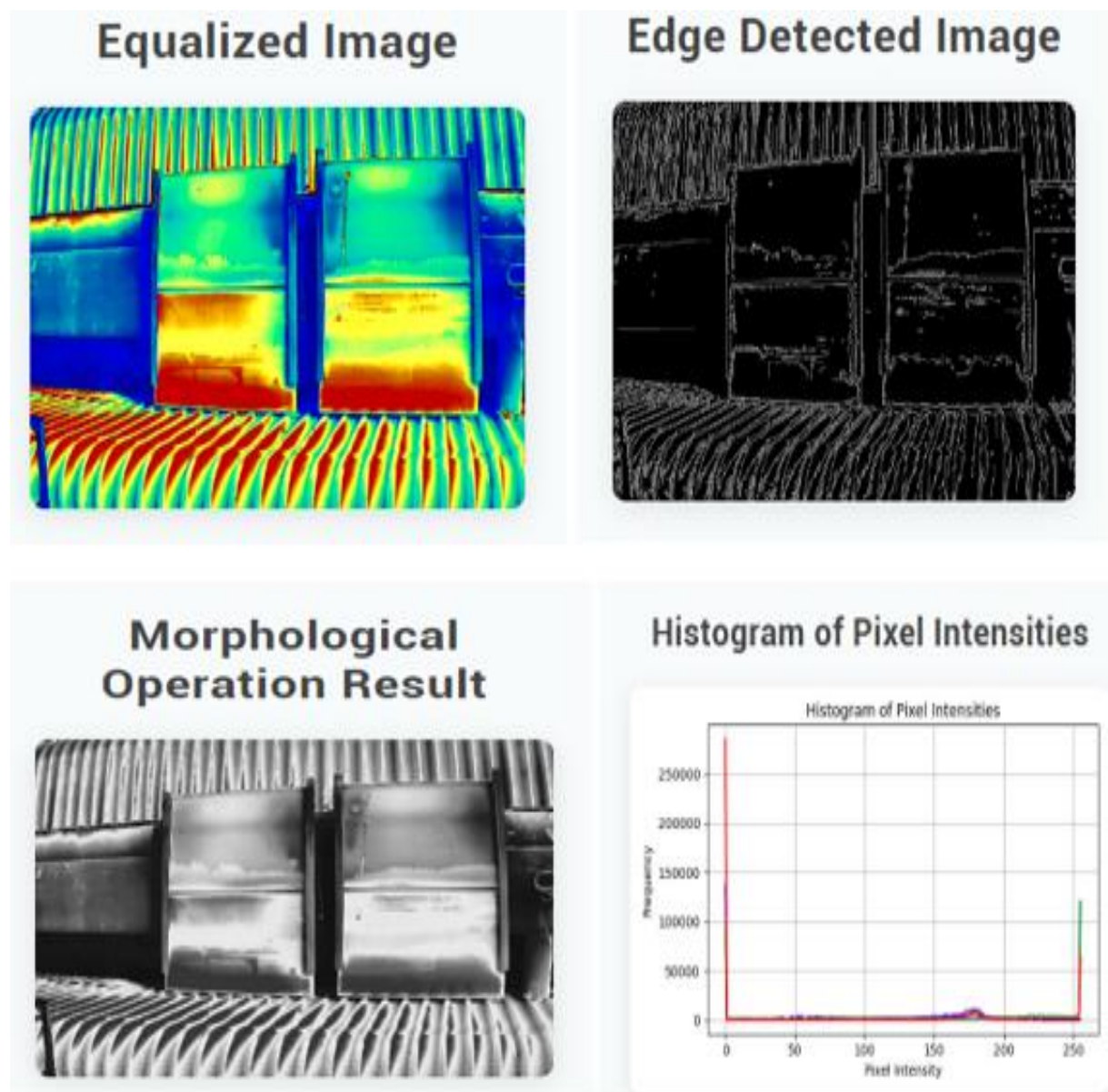


Figure 15. Application of morphological transformation known as "Closing" within the fault detection process.

The Simple Linear Iterative Clustering (SLIC) algorithm is a popular method for superpixel generation. Superpixels are groups of pixels that share similar characteristics, effectively reducing the complexity of image processing tasks by working on clusters of pixels rather than individual pixels. SLIC is especially useful in segmenting images into meaningful regions based on color and spatial proximity. SLIC algorithm and its impact are illustrated in Figure 16.

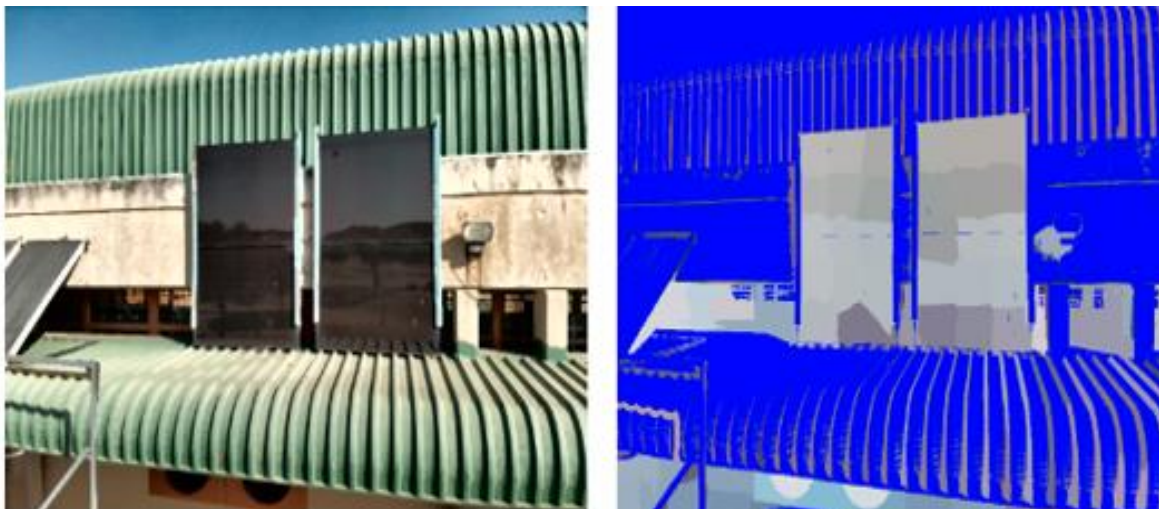


Figure 16.
Explanation of the SLIC algorithm and its impact on the project.

Throughout this research, several critical observations and advancements were made which are on a par with the best results ever obtained in this area of research [13, 26-29]. The deployment of drones facilitated the collection of high-resolution images, providing detailed visual and thermal data crucial for identifying anomalies such as hot pixels, cell cracks, and delamination in PV modules. The use of various image preprocessing techniques such as Box blur, Gaussian blur, Median blur, and Histogram equalization proved effective in enhancing image quality, which is paramount for accurate fault detection. Furthermore, the application of unsupervised machine learning algorithms enabled the autonomous detection of faults without the need for pre-labeled data. Techniques such as clustering and anomaly detection were instrumental in distinguishing between normal and faulty conditions. This approach not only reduced the dependency on expert supervision but also minimized human error, leading to more reliable and consistent fault detection outcomes [30].

The integration of machine vision with thermal imaging also played a pivotal role in enhancing the detection of temperature anomalies, which are often indicative of potential faults. By analyzing thermal patterns and correlating them with visual data, the system was able to identify subtle defects that might otherwise be overlooked. This multimodal analysis provided a more holistic understanding of the health and performance of PV modules. The findings of this research underscore the immense potential of leveraging drones and machine vision for unsupervised fault detection in large PV systems. The automated nature of this approach not only improves the efficiency of fault detection but also significantly reduces operational costs and downtime. As the demand for renewable energy continues to grow, ensuring the optimal performance and longevity of PV systems becomes increasingly critical. The methodologies and technologies explored in this study offer a robust framework for advancing the maintenance and monitoring of solar installations. The original dataset employed in this work is publicly and freely available for scientific community use at <https://doi.org/10.17632/5ssmfjgrpc.1> [26].

5. Conclusions

Automated fault detection and analysis for large PV systems using PV module fault detection in drone vision system has been presented in this study. The integration of drones and machine vision for unsupervised fault detection represents a significant leap forward in the management of PV systems. By harnessing the power of these technologies, we can enhance the sustainability and efficiency of solar energy production, contributing to a more resilient and environmentally friendly energy infrastructure. Our future research would focus on refining these techniques and exploring their applicability across

different types of renewable energy systems, paving the way for a smarter and more sustainable energy future.

Transparency:

The authors confirm that the manuscript is an honest, accurate, and transparent account of the study; that no vital features of the study have been omitted; and that any discrepancies from the study as planned have been explained. This study followed all ethical practices during writing.

Acknowledgement:

The authors received funding from the Tshwane University of Technology, South Africa.

Copyright:

© 2025 by the authors. This open-access article is distributed under the terms and conditions of the Creative Commons Attribution (CC BY) license (<https://creativecommons.org/licenses/by/4.0/>).

References

- [1] Q. Hassan *et al.*, "The renewable energy role in the global energy Transformations," *Renewable Energy Focus*, vol. 48, p. 100545, 2024. <https://doi.org/10.1016/j.ref.2024.100545>
- [2] L. Melnyk, O. Derykolenko, Y. Mazin, O. Matsenko, and V. Piven, "Modern trends in the development of renewable energy: The experience of the EU and leading countries of the world," *Mechanism of an Economic Regulation*, vol. 3, no. 89, pp. 117-133, 2020. <https://doi.org/10.21272/mer.2020.89.117>
- [3] U. Hijjawi, S. Lakshminarayana, T. Xu, G. P. M. Fierro, and M. Rahman, "A review of automated solar photovoltaic defect detection systems: Approaches, challenges, and future orientations," *Solar Energy*, vol. 266, p. 112186, 2023. <https://doi.org/10.1016/j.solener.2023.07.037>
- [4] A. K. V. De Oliveira, M. Aghaei, and R. R  ther, "Automatic inspection of photovoltaic power plants using aerial infrared thermography: A review," *Energies*, vol. 15, no. 6, p. 2055, 2022. <https://doi.org/10.3390/en15062055>
- [5] W. Tang, Q. Yang, Z. Dai, and W. Yan, "Module defect detection and diagnosis for intelligent maintenance of solar photovoltaic plants: Techniques, systems and perspectives," *Energy*, p. 131222, 2024. <https://doi.org/10.1016/j.energy.2024.131222>
- [6] N. M. Kumar *et al.*, "Solar PV module technologies," in *Photovoltaic Solar Energy Conversion*: Elsevier. <https://doi.org/10.1016/B978-0-12-819069-2.00003-2>, 2020, pp. 51-78.
- [7] I. Hoiaas, K. Grujic, A. G. Imenes, I. Burud, E. Olsen, and N. Belbachir, "Inspection and condition monitoring of large-scale photovoltaic power plants: A review of imaging technologies," *Renewable and Sustainable Energy Reviews*, vol. 161, p. 112353, 2022. <https://doi.org/10.1016/j.rser.2022.112353>
- [8] G. R. Venkatakrisnan *et al.*, "Detection, location, and diagnosis of different faults in large solar PV systems—a review," *International Journal of Low-Carbon Technologies*, vol. 18, pp. 659-674, 2023. <https://doi.org/10.1093/ijlct/ctad050>
- [9] G. Tanda and M. Migliazzi, "Infrared thermography monitoring of solar photovoltaic systems: A comparison between UAV and aircraft remote sensing platforms," *Thermal Science and Engineering Progress*, vol. 48, p. 102379, 2024. <https://doi.org/10.1016/j.tsep.2024.102379>
- [10] D. Vijayalakshmi, M. K. Nath, and O. P. Acharya, "A comprehensive survey on image contrast enhancement techniques in spatial domain," *Sensing and Imaging*, vol. 21, no. 1, p. 40, 2020. <https://doi.org/10.1007/s11220-020-00219-5>
- [11] Y.-Y. Hong and R. A. Pula, "Methods of photovoltaic fault detection and classification: A review," *Energy Reports*, vol. 8, pp. 5898-5929, 2022. <https://doi.org/10.1016/j.egy.2022.04.043>
- [12] M. Jalal, I. U. Khalil, and A. ul Haq, "Deep Learning approaches for visual faults diagnosis of photovoltaic systems: State-of-the-art review," *Results in Engineering*, p. 102622, 2024. <https://doi.org/10.1016/j.rineng.2024.102622>
- [13] M. Alsafasfeh, I. Abdel-Qader, B. Bazuin, Q. Alsafasfeh, and W. Su, "Unsupervised fault detection and analysis for large photovoltaic systems using drones and machine vision," *Energies*, vol. 11, no. 9, p. 2252, 2018. <https://doi.org/10.3390/en11092252>
- [14] Z. Didi and I. El Azami, "Improved performance of photovoltaic panels by image processing," presented at the International Conference on Big Data and Internet of Things, Cham: Springer International Publishing, 2022.
- [15] S. Jumaboev, D. Jurakuziev, and M. Lee, "Photovoltaics plant fault detection using deep learning techniques," *Remote Sensing*, vol. 14, no. 15, p. 3728, 2022. <https://doi.org/10.3390/rs14153728>
- [16] Z. B. Duranay, "Fault detection in solar energy systems: A deep learning approach," *Electronics*, vol. 12, no. 21, p. 4397, 2023. <https://doi.org/10.3390/electronics12214397>

- [17] S. P. Pathak, S. Patil, and S. Patel, "Solar panel hotspot localization and fault classification using deep learning approach," *Procedia Computer Science*, vol. 204, pp. 698-705, 2022. <https://doi.org/10.1016/j.procs.2022.08.084>
- [18] A. Greco, C. Pironti, A. Saggese, and M. V. Vento, V., "A deep learning-based approach for detecting panels in photovoltaic plants," in *Proceedings of the 3rd International Conference on Applications of Intelligent Systems*, 2020, pp. 1-7, doi: <https://doi.org/10.1109/ICAIS50574.2020.9297345>.
- [19] N. V. Sridharan and V. Sugumaran, "Convolutional neural network based automatic detection of visible faults in a photovoltaic module," *Energy Sources, Part A: Recovery, Utilization, and Environmental Effects*, pp. 1-16, 2021. <https://doi.org/10.1080/15567036.2021.1979890>
- [20] B. Kim, R. O. Serfa Juan, D.-E. Lee, and Z. Chen, "Importance of image enhancement and CDF for fault assessment of photovoltaic module using IR thermal image," *Applied Sciences*, vol. 11, no. 18, p. 8388, 2021. <https://doi.org/10.3390/app11188388>
- [21] R.-W. Bello, P. A. Owolawi, E. A. van Wyk, and C. Du, "SAM-PIE: SAM-Enabled photovoltaic-module image enhancement for fault inspection and analysis using ResNet50 and CNNs," *International Journal of Advanced Computer Science & Applications*, vol. 15, no. 11, pp. 333-341, 2024. <https://doi.org/10.14569/IJACSA.2024.0151146>
- [22] B. Sekeroglu and K. Tuncal, *Image processing in unmanned aerial vehicles. In Unmanned Aerial Vehicles in Smart Cities*. Springer. https://doi.org/10.1007/978-3-030-41723-4_9, 2020.
- [23] R. Sarabia, A. Aquino, J. M. Ponce, G. López, and J. M. Andújar, "Automated identification of crop tree crowns from uav multispectral imagery by means of morphological image analysis," *Remote Sensing*, vol. 12, no. 5, p. 748, 2020. <https://doi.org/10.3390/rs12050748>
- [24] E. A. Sekehravani, E. Babulak, and M. Masoodi, "Implementing canny edge detection algorithm for noisy image," *Bulletin of Electrical Engineering and Informatics*, vol. 9, no. 4, pp. 1404-1410, 2020. <https://doi.org/10.11591/eei.v9i4.1033>
- [25] Y. Li and B. Liu, "Improved edge detection algorithm for canny operator," in *2022 IEEE 10th Joint International Information Technology and Artificial Intelligence Conference (ITAIIC)*. <https://doi.org/10.1109/ITAIIC55431.2022.9903300>, 2022, vol. 10: IEEE, pp. 1-5.
- [26] R.-W. Bello, P. A. Owolawi, E. A. van Wyk, and C. Du, "Photovoltaic module dataset for automated fault detection and analysis in large photovoltaic systems using photovoltaic module fault detection," *Data in Brief*, vol. 57, p. 111184, 2024. <https://doi.org/10.17632/5ssmfpgprc.1>
- [27] G. B. Balachandran, M. Devisridhiyadharshini, M. E. Ramachandran, and R. Santhiya, "Comparative investigation of imaging techniques, pre-processing and visual fault diagnosis using artificial intelligence models for solar photovoltaic system—A comprehensive review," *Measurement*, vol. 232, p. 114683, 2024. <https://doi.org/10.1016/j.measurement.2024.114683>
- [28] K. Osmani, A. Haddad, T. Lemenand, B. Castanier, M. Alkhdher, and M. Ramadan, "A critical review of PV systems' faults with the relevant detection methods," *Energy Nexus*, p. 100257, 2023. <https://doi.org/10.1016/j.nexus.2023.100257>
- [29] S. Hassan and M. Dhimish, "Enhancing solar photovoltaic modules quality assurance through convolutional neural network-aided automated defect detection," *Renewable Energy*, vol. 219, p. 119389, 2023. <https://doi.org/10.1016/j.renene.2023.01.069>
- [30] G. M. El-Banby, N. M. Moawad, B. A. Abouzalm, W. F. Abouzaid, and E. Ramadan, "Photovoltaic system fault detection techniques: A review," *Neural Computing and Applications*, vol. 35, no. 35, pp. 24829-24842, 2023. <https://doi.org/10.1007/s00542-023-08404-9>